Chloroform-Enhanced Incorporation of Hydrophobic Gold Nanocrystals into Dioleoylphosphatidylcholine (DOPC) Vesicle Membranes

Michael R. Rasch, Yixuan Yu, Christian Bosoy, Brian W. Goodfellow, Brian A. Korgel*

Department of Chemical Engineering, Texas Materials Institute, Center for Nano and Molecular Science and Technology, The University of Texas at Austin, Austin, Texas 78712-1062, USA

*Corresponding author: korgel@che.utexas.edu; (T) +1-512-471-5633; (F) +1-512-471-7060

Supporting Information

Dynamic Light Scattering data anlaysis. In DLS, the instrument measures the correlation in light scattering intensity over time and reports the data as the intensity autocorrelation function given by Eqn (S-1).[39,40] For each dispersion, $g_2(t)$ was measured in triplicate.

$$g_2(t) = \frac{\langle I(t)I(0)\rangle}{\langle I(0)\rangle^2} \quad \text{(S-1)}$$

The intensity autocorrelation function $g_2(t)$, is related to the electric field autocorrelation function $g_1(t)$ by the Siegert relationship, equation 6.[39]

$$g_2(t) = 1 + \beta \cdot |g_1(t)|^2 \quad \text{(S-2)}$$

β is a constant. Each scattering particle contributes a single exponential decay to the correlation in light scattering intensity, thus the general form of $g_1(t)$ is the following:

$$g_1(t) = \sum_{i=1}^{m} A_i e^{-\Gamma_i \cdot t} \quad \text{(S-3)}$$

In Eqn (S-3), each particle size (i) has a constant pre-exponential term A_i and a scattering intensity decay rate Γ_i. Equation 8 shows how the decay rate is related to the scattering vector q and the particle diffusion coefficient D_i. Also, Eqn (S-4) employs the Stokes-Einstein relationship to relate the decay rate directly to the particle hydrodynamic diameter d_i.[39] The refractive index n, of water is 1.333, the dynamic viscosity η of water at 25°C is 0.89 cP, k is Boltzmann's constant, and T is temperature (298 K).

$$\Gamma_i = q^2 \cdot D_i = \left(\frac{4n}{\lambda}\sin\left(\frac{\theta}{2}\right)\right)^2 \cdot \left(\frac{kT}{3\eta \cdot d_i}\right) \quad \text{(S-4)}$$

The particle size is obtained by fitting Eqns (S2-S4) to the experimental $g_2(t)$. The DLS data were well represented by assuming only two particle sizes, so that $m = 2$ in Eqn (S3).[41,42] In this

case, the two pre-exponentials represent the relative amplitude of scattering from each particle size such that $A_1 + A_2 = 1$.[43,44]

Eqns (S2-S4) were fit to three replicate measurements of $g_2(t)$ using non-linear least squares regression, assuming only non-negative solutions were valid, minimizing χ^2:

$$\chi^2 = \sum \left(g_2(t)\big|_{\exp} - g_2(t)\big|_{\mathrm{mod}\,el} \right)^2 \qquad \text{(S-5)}$$

For each dispersion, DLS was performed by taking three replicate measurements of the light scattering intensity correlation function (g_2), which is related to the intensity of scattered light $I(\tau)$ according to Eqn (S-1). DLS data were fit to a light scattering modeling derived from Eqns (S2-S3) by assuming that the scattering population consists of two different particle sizes (i = I, II) with pre-exponential constants A_i, and size-dependent constants Γ_i, that correspond to the relaxation rate of the light scattering intensity given in Eqn (S-4):[41-43]

$$g_2(\tau) - 1 = \beta \cdot \left[A_I \exp\left(-\Gamma_I \cdot \tau\right) + A_{II} \cdot \exp\left(-\Gamma_{II} \cdot \tau\right) \right]^2 \qquad \text{(S-6)}$$

Tables S1 and S2 provide the best fit parameters to the DLS data in Figure 11 in the main body of the paper. Figures S1 and S2 show more DLS data and the fits. Figure S3 shows a comparison of χ^2 values obtained when fitting the DLS data with a unimodal and bimodal size distribution. The bimodal size distribution always gave the better model fit to the data. The values in Table S2 are the ones use to fit the DLS data in Figure 11 in the main body of the paper.

Table S1. DLS fitting parameters using a unimodal size distribution.

Sample Number	Gold Core Size (nm)	Annealing Condition	Step of Dispersing	d (nm)	β	Γ (ms^{-1})	χ^2
1	1.8	No Anneal	Sonicated	5151	0.461	0.066	0.1591
2	1.8	No Anneal	Centrifuged	162	0.841	2.108	0.0461
3	1.8	No Anneal	Extruded	92	0.883	3.006	0.0044
4	1.8	Anneal, then vacuum	Sonicated	1918	0.546	0.179	0.5665
5	1.8	Anneal, then vacuum	Centrifuged	135	0.890	2.533	0.0166
6	1.8	Anneal, then vacuum	Extruded	91	0.901	3.766	0.0064
7	1.8	Vacuum, then anneal	Sonicated	293	0.773	1.168	0.0665
8	1.8	Vacuum, then anneal	Centrifuged	170	0.806	2.011	0.0211
9	1.8	Vacuum, then anneal	Extruded	121	0.888	2.833	0.0131
10	4.1	No Anneal	Sonicated	1354	0.464	0.253	0.2466
11	4.1	No Anneal	Centrifuged	131	0.910	2.620	0.0150
12	4.1	No Anneal	Extruded	107	0.882	3.214	0.0118
13	4.1	Anneal, then vacuum	Sonicated	2257	0.503	0.152	0.2429
14	4.1	Anneal, then vacuum	Centrifuged	125	0.924	2.730	0.0121
15	4.1	Anneal, then vacuum	Extruded	104	0.931	3.287	0.0075
16	4.1	Vacuum, then anneal	Sonicated	341	0.506	1.003	0.0197
17	4.1	Vacuum, then anneal	Centrifuged	193	0.673	1.771	0.0183
18	4.1	Vacuum, then anneal	Extruded	138	0.701	2.477	0.0029

Table S2. DLS fitting parameters using a bimodal size distribution. The sample numbers and descriptions correspond to those in Table S1.

Sample Number	Amplitude wt. diameter* (nm)	d_1 (nm)	d_2 (nm)	A_1	A_2	β	Γ_1 (ms^{-1})	Γ_2 (ms^{-1})	χ^2
1	8097	748	10088	0.213	0.787	0.474	0.458	0.034	0.0232
2	223	89	357	0.499	0.501	0.851	3.856	0.960	0.0111
3	96	32	102	0.082	0.918	0.887	8.540	2.709	0.0014
4	3916	210	5231	0.262	0.738	0.578	1.630	0.065	0.0603
5	151	49	172	0.172	0.828	0.899	6.947	1.990	0.0019
6	97	34	105	0.116	0.884	0.907	9.994	3.263	0.0015
7	395	108	527	0.315	0.685	0.785	3.175	0.650	0.0065
8	197	65	234	0.217	0.783	0.815	5.290	1.465	0.0025
9	131	43	145	0.132	0.868	0.896	8.020	2.368	0.0042
10	3174	304	4767	0.357	0.643	0.481	1.128	0.072	0.0259
11	144	50	164	0.170	0.830	0.918	6.813	2.090	0.0032
12	121	59	155	0.352	0.648	0.889	5.801	2.206	0.0025
13	3839	451	5102	0.272	0.728	0.517	0.759	0.067	0.0976
14	137	50	155	0.169	0.831	0.931	6.790	2.208	0.0025
15	114	53	133	0.242	0.758	0.937	6.416	2.574	0.0014
16	449	144	610	0.344	0.656	0.512	2.384	0.561	0.0016
17	236	90	308	0.331	0.669	0.680	3.821	1.111	0.0027
18	144	43	151	0.064	0.936	0.704	7.891	2.268	0.0011

*****Amplitude weighted diameter = $A_1d_1 + A_2d_2$

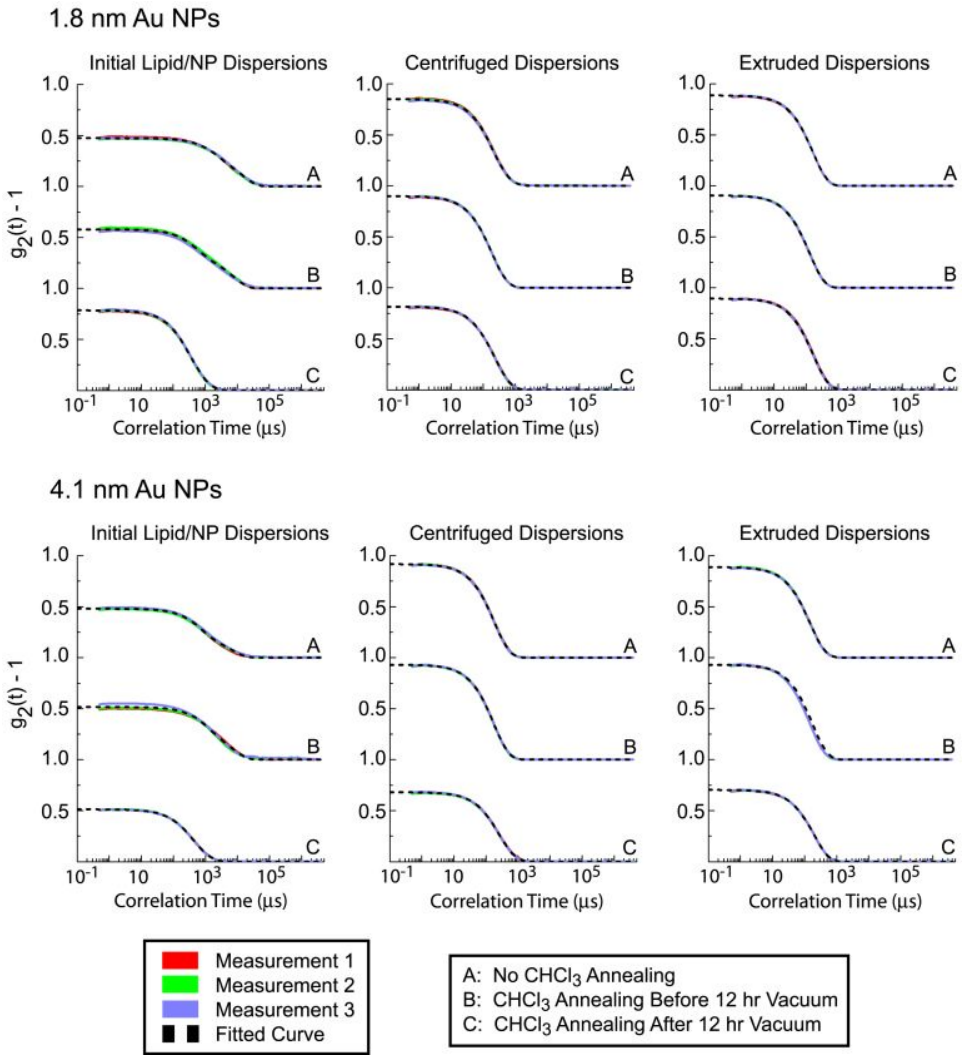

Figure S1. DLS data for each lipid/Au nanocrystal dispersion fit to the light scattering model described in the main body of the paper using the parameters listed in Table S2. The Au nanocrystals are capped with dodecanethiol. The fitted curves are plotted in Figure 11 of the main body of the paper.

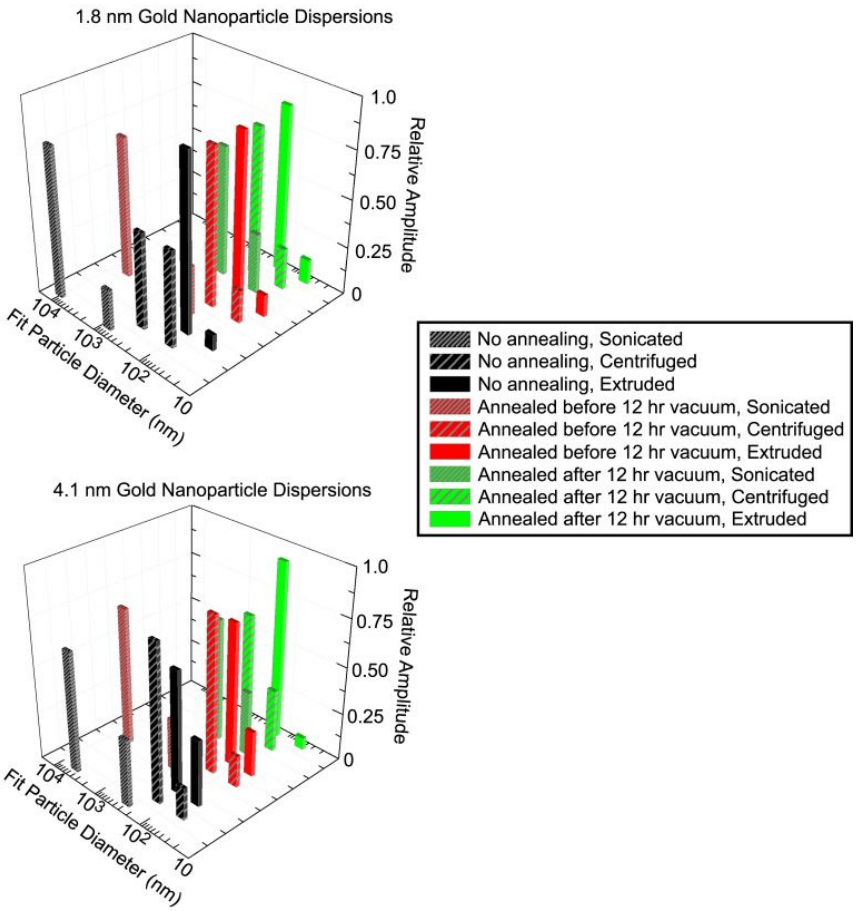

Figure S2. DLS fitting results plotted as fitted particle diameter versus the scattering amplitude using the parameters in Table S2. The Au nanocrystals were capped with dodecanethiol.

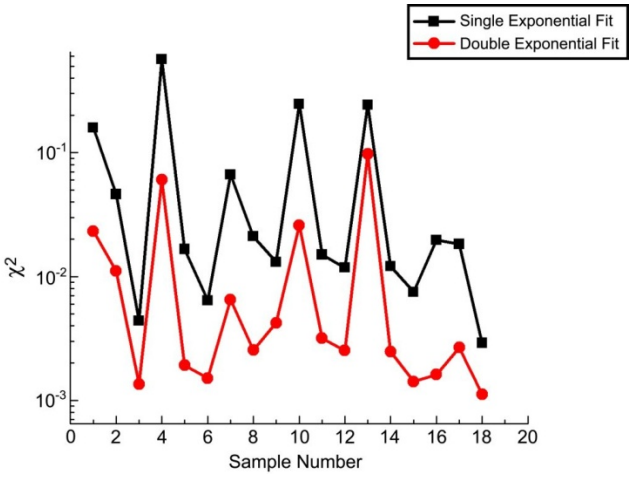

Figure S3. Least squares fit parameters (χ^2) of two different DLS models, a single exponential (one particle size) and a double exponential (two particle sizes), fit to the data in Figure 11 in the main body of the paper. Tables S1 and S2 list the parameters used to fit the two models to the data. The double exponential model was always found to provide the best fit. The sample numbers refer to the entries in column 1 of Table 2.

Figure S4 shows nanocrystal/lipid films dried at various conditions. Microphase separation between the nanocrystals and lipid was observed in all cases. Chloroform vapor annealing led to mixing of the nanocrystals in the lipid films, as shown in Figure S5. Vacuum-drying the chloroform-annealed nanocrystal/lipid films did not lead to phase segregation of the nanocrystals. These films, however, did not contain residual chloroform and nanocrystals were not observed to load the vesicle membranes significantly.

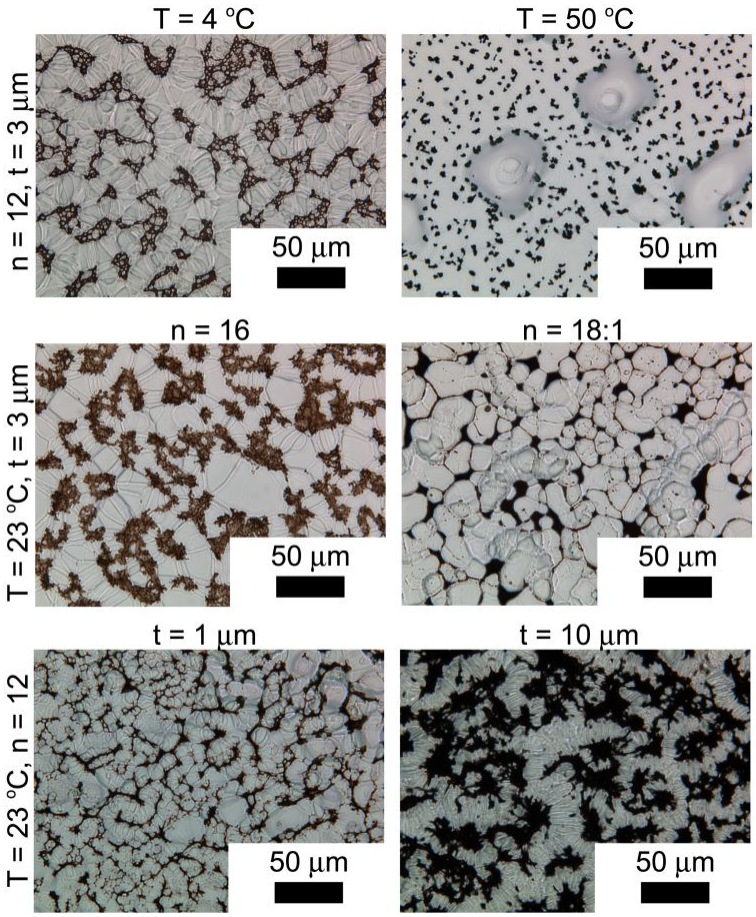

Figure S4. Varying the drying conditions for films of DOPC and 1.8 nm core diameter gold nanocrystals drop cast on glass from a chloroform dispersion. The drying variables included temperature (T), number of carbon atoms per thiol ligand (n = 12 for dodecanethiol, n = 16 for hexadecanethiol, n = 18:1 for 9-octadecene-1-thiol), and average film thickness (t). The drying temperature was varied by drop-casting the dispersions in either a cold room (4°C) or an oven (50°C) at atmospheric pressure, after equilibrating the coverglass and dispersion at the drop-cast temperature for 10 minutes. In each test, 0.3 mg of nanocrystals was added for each 1 mg of lipid.

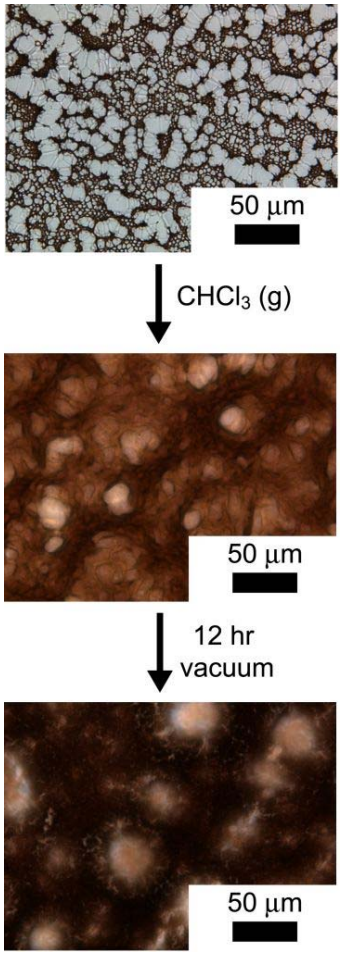

Figure S5. Chloroform vapor-annealed DOPC-nanocrystal films do not phase segregate when placed under vacuum after annealing. At 40x magnification, the annealed films appear homogeneous before and after vacuum.

Other solvents were tested for vapor-annealing. As shown in Figure S6, only dichloromethane led to mixing of the nanocrystals in the lipid films. CryoTEM images of DOPC vesicles formed with nanocrystals after dichloromethane vapor-annealing are shown in Figure S7—dichloromethane annealing also helped nanocrystal loading of DOPC vesicle membranes.

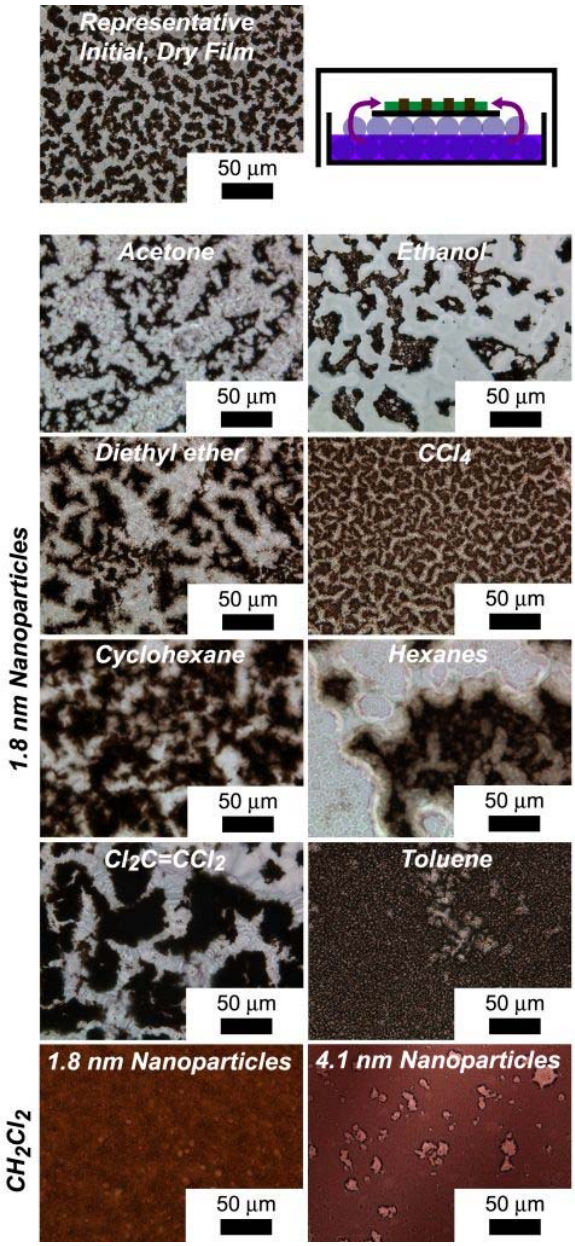

Figure S6. Dried films of DOPC and dodecanethiol-coated 1.8 nm diameter Au nanocrystals exposed to various solvent vapor. The sketch at the top right illustrates the solvent vapor annealing apparatus, with purple arrows indicating the diffusion of solvent vapor to the film from the underlying liquid phase. Only toluene and dichloromethane vapor exposure led to significant mixing of lipid and nanocrystals.

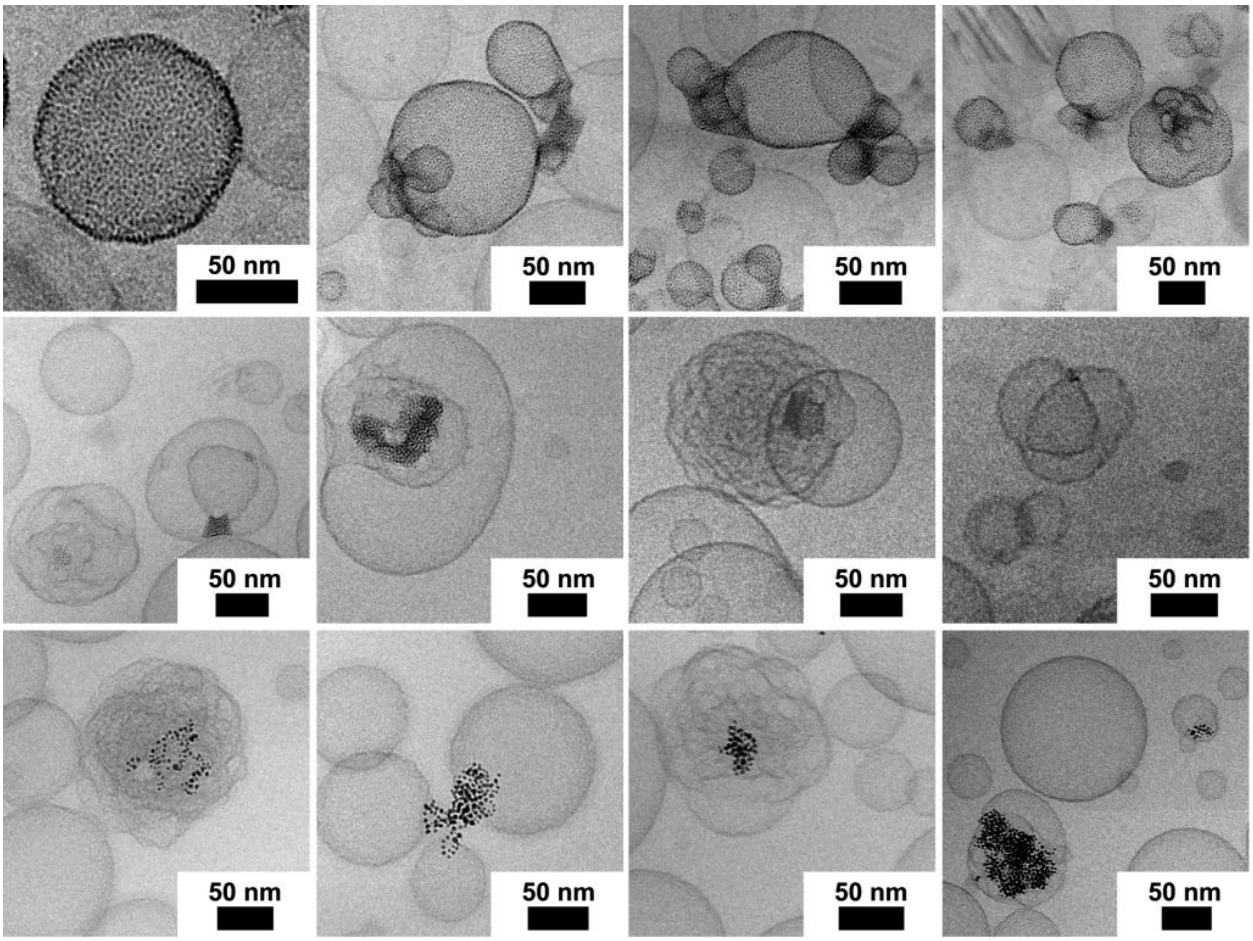

Figure S7. CryoTEM images of DOPC vesicles formed with Au nanocrystals after annealing the dried lipid/nanocrystal films with dichloromethane. Top row: dodecanethiol-coated 1.8 nm nanoparticles, middle row: hexadecanethiol-coated 1.8 nm nanoparticles, bottom row: dodecanethiol-coated 4.1 nm nanoparticles.

Figure S8 shows ^{1}H and ^{31}P NMR spectra for DOPC vesicles with and without Au nanocrystals and with and without chloroform vapor-annealing. The $CHCl_3$ proton resonance (7.6 ppm) is absent in the ^{1}H spectrum of A as expected since the sample was not $CHCl_3$ vapor-annealed. Sample B is DOPC in D_2O after $CHCl_3$ vapor-annealing. For sample B, the $CHCl_3$ proton resonance is detectable in the ^{1}H spectrum, and the chloroform to lipid molar ratio is 0.75 based on the area of the chloroform ^{1}H peak (1.14 area) divided by the area of the choline methyl ^{1}H peak at 3.15 ppm (13.71 area ÷ 9 methyl protons per choline). The ^{31}P peak is broadened in B relative to A, which suggests that chloroform may enhance DOPC ordering. Sample C was prepared by dispersing DOPC with dodecanethiol-coated 1.8 nm nanoparticles after $CHCl_3$ vapor-annealing. The area of the chloroform resonance peak in the ^{1}H NMR spectrum of C is 0.39 and the area of the choline head group resonance peak is 3.38, so the molar ratio of DOPC to chloroform in the dispersion is 1.0. In the ^{31}P spectrum, the resonance peak is significantly broadened relative to samples A and B. The ^{31}P line width for C is about 200% larger, so it appears that nanocrystals lead to slower lipid diffusion or more lipid order. Sample D was re-extruded after NMR. The chloroform proton resonance peak area was 0.077 for sample D,

which corresponded to a chloroform to lipid molar ratio of 0.2. The ^{31}P peak line width only differed from C by 10%.

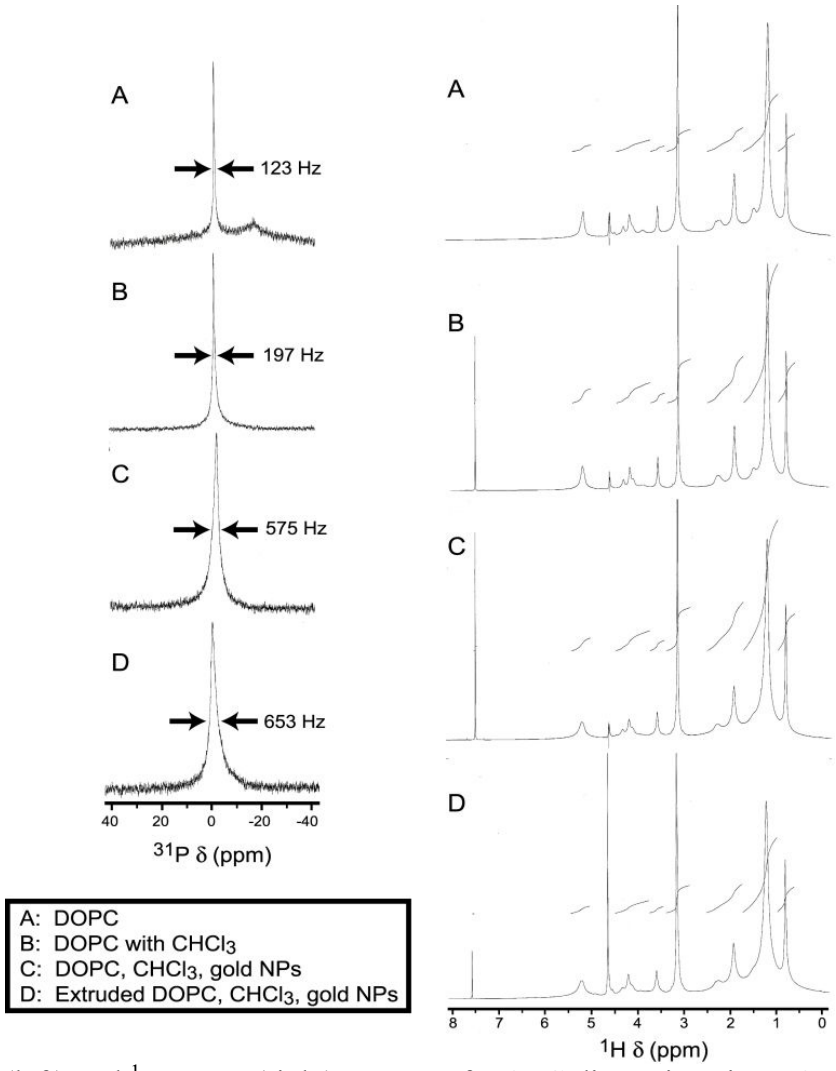

Figure S8. ^{31}P (left) and ^{1}H NMR (right) spectra of DOPC dispersions in D_2O with and without dodecanethiol-coated 1.8 nm gold nanocrystals (NPs). Sample A was not prepared with chloroform vapor annealing, while B-D were prepared with chloroform vapor annealing. The full width at half maximum is indicated for the peak in each ^{31}P spectrum.

Figure S9 shows optical UV-visible absorbance spectra of the Au nanocrystals.

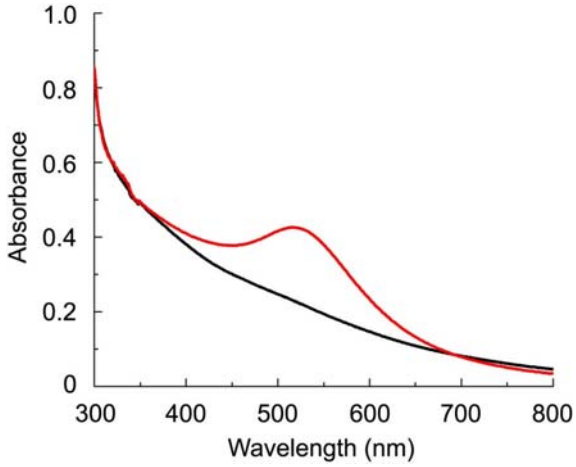

Figure S9. UV-visible absorbance spectra of gold nanocrystals used in the study. The black line is 1.8 nm gold nanocrystals and the red line is 4.1 nm gold nanocrystals. The spectra for the 1.8 nm gold nanocrystals coated with dodecanethiol and hexadecanethiol are identical.